AGU PUBLICATIONS

JGR

Journal of Geophysical Research: Atmospheres

RESEARCH ARTICLE
10.1002/2015JD024269

Key Points:
- In-depth analyses of the attachment process of triggered lightning dart-stepped leaders
- Lengths, speeds, and durations of the upward connecting positive leader are measured and calculated
- Observed time delay between d*E*/d*t* and d*I*/d*t* peaks confirms existence of elevated junction point

Correspondence to:
J. D. Hill,
jonathan.d.hill@nasa.gov

Citation:
Hill, J. D., M. A. Uman, D. M. Jordan, T. Ngin, W. R. Gamerota, J. Pilkey, and J. Caicedo (2016), The attachment process of rocket-triggered lightning dart-stepped leaders, *J. Geophys. Res. Atmos.*, *121*, doi:10.1002/2015JD024269.

Received 24 SEP 2015
Accepted 3 JAN 2016
Accepted article online 7 JAN 2016

The attachment process of rocket-triggered lightning dart-stepped leaders

J. D. Hill[1,2], M. A. Uman[1], D. M. Jordan[1], T. Ngin[1,3], W. R. Gamerota[1,4], J. Pilkey[1,5], and J. Caicedo[1]

[1]Department of Electrical and Computer Engineering, University of Florida, Gainesville, Florida, USA, [2]Now at Stinger Ghaffarian Technologies, Kennedy Space Center, Florida, USA, [3]Now at Leidos, Inc., Arlington, Virginia, USA, [4]Now at IBM Business Performance Services, Armonk, New York, USA, [5]Now at Sandia National Laboratories, Albuquerque, New Mexico, USA

Abstract Time-correlated 1.54 μs high-speed video frames, channel-base current and current derivative (d*I*/d*t*), and electric field derivative (d*E*/d*t*) measurements are used to analyze the attachment process of triggered lightning dart-stepped leaders. Lengths, speeds, and durations of the upward-connecting positive leaders propagating from the launching structure are measured and calculated. The "leader burst" occurring immediately preceding the d*E*/d*t* slow front is demonstrated to be a distinctly different process from the preceding downward dart-stepped leader steps and is associated with the fast increase in channel-base current due to the initial interactions of the downward and upward leader streamer zones. Locations of the leader burst pulses are found to occur within or immediately above the connection region. Pulses superimposed on the d*E*/d*t* slow front are shown to occur after the initial connection between the downward and upward leaders and are associated with kiloampere-scale increases in the channel-base current. Subsequent fast-transition pulses are found to produce multiple kiloampere-scale increases in the channel-base current. Observed time delays between d*E*/d*t* and d*I*/d*t* peaks for slow front and fast-transition pulses confirm the existence of an elevated junction point between the downward and upward leaders. Average downward current wave speeds for fast-transition pulses are found to be a factor of 2 to 2.5 faster than those for slow-front pulses. For 51 dart-stepped leader events, the average total duration of the attachment process, starting with the initial fast current increase and ending with the peak of the final d*I*/d*t* fast-transition pulse, is measured to be 1.77 μs.

1. Introduction

Much of the published research conducted at the International Center for Lightning Research and Testing (ICLRT) during the past seven years has focused on the physics and mechanisms of low-altitude, negative polarity lightning leader propagation and the associated electromagnetic emissions from electrostatic to gamma radiation [e.g., *Biagi et al.*, 2009, 2010, 2014; *Dwyer et al.*, 2003, 2004, 2005, 2011; *Gamerota et al.*, 2014a, 2014b, 2015; *Hill et al.*, 2011, 2012; *Howard et al.*, 2008, 2010, 2011; *Saleh et al.*, 2009; *Schaal et al.*, 2013, 2014]. The ICLRT is a facility jointly operated by the University of Florida and the Florida Institute of Technology and is located about 45 km northeast of Gainesville, FL. The ICLRT is one of only two sites in the United States and four in the world where lightning is presently artificially initiated ("triggered") using the rocket-and-wire technique. Coordinated high-speed video, radio-frequency electromagnetic field, and energetic radiation (X-rays and gamma rays) measurements of triggered and natural lightning leaders propagating at low altitude have allowed ICLRT researchers to gain better understanding of the leader step formation process [e.g., *Biagi et al.*, 2009, 2010, 2014; *Gamerota et al.*, 2014a, 2014b, 2015; *Hill et al.*, 2011; *Howard et al.*, 2010, 2011] and the related high-energy emissions [e.g., *Dwyer et al.*, 2003, 2004, 2005, 2011; *Hill et al.*, 2012; *Howard et al.*, 2008, 2010; *Saleh et al.*, 2009; *Schaal et al.*, 2013, 2014]. Most of these studies have concentrated on the time period extending from several microseconds to several hundred microseconds prior to the return stroke when the propagating leaders are within about 500 m of ground. There is a relative paucity of literature regarding the attachment process, which occurs in the microseconds immediately prior to the return stroke. The attachment process is comparatively difficult to study due to the complexity of the physical processes confined to both a relatively small spatial and temporal window.

Triggered lightning provides a convenient method for studying the attachment process due to its repeatability and to the fact that the attachment point can be controlled with a high degree of certainty. *Rakov and Uman* [2003], ch.7] provide a detailed description of the triggered lightning process. While capturing a sizable data set of close-range, high-speed optical, and electromagnetic measurements of the natural lightning

attachment process, particularly for first strokes preceded by stepped leaders, to ground or low-altitude grounded structures would be extremely important to understanding natural lightning attachment, doing so in a timely manner is simply impractical considering the random nature of natural lightning. Triggered lightning return strokes are frequently preceded by dart-stepped leaders that, while not a direct proxy for natural stepped leaders, have sufficiently similar propagation characteristics to be used as an effective study tool.

For triggered lightning strokes, the attachment process can be generally defined as the interaction of the negatively charged, downward propagating leader with the grounded metallic launching structure that ultimately leads to the initiation of the upward-propagating return stroke current wave and the subsequent net transfer of negative charge to Earth. In this paper, the attachment process is specifically defined to extend from the observed initial rapid increase in channel-base current at the end of the upward connecting positive leader (UCPL) propagation to the time of the final current pulse that establishes the full connection between the downward and upward propagating leaders as measured by the peak d*I*/d*t*. Some authors include the time of the UCPL propagation in the attachment process. We do not but determine that time separately. For natural first strokes, the attachment process always includes an interaction between the downward negative stepped leader and one or more upward propagating positively charged leaders originating from the ground or grounded objects/structures. One or more UCPLs connect to the downward stepped leader. Upward propagating leaders initiating from the ground are often several tens of meters in length, while those initiating from elevated structures (communications towers, tall buildings, etc.) can extend many hundreds of meters. High-speed photographs of UCPLs occurring in response to natural downward negative stepped leaders have been recently published by *Gao et al*. [2014], *Jiang et al*. [2014], *Lu et al*. [2013], *Petersen and Beasley* [2013], *Tran et al*. [2014], and *Warner* [2010], among others. UCPLs associated with natural cloud-to-ground subsequent strokes have been inferred to exist [e.g., *Orville and Idone*, 1982], although no definitive images appear in the published literature. UCPLs associated with triggered lightning return strokes, which are similar to natural lightning subsequent strokes, were first imaged by *Wang et al*. [1999] using the Automatic Lightning Progressing Feature Observation System (ALPS) photodiode imaging system. For one triggered lightning leader, *Wang et al*. [1999] observed a UCPL with length of 7–11 m, duration of several hundred nanoseconds, and speed of 2.0×10^7 m/s. *Biagi et al*. [2009] presented the first digital high-speed video images of UCPLs associated with triggered lightning return strokes. For an eight stroke flash, *Biagi et al*. [2009] imaged UCPLs ranging from about 8 m to 22 m in length. Each frame exposure time was 20 μs.

Electric and magnetic field waveforms of the attachment processes of natural first and subsequent strokes have typically been studied at distances of several tens of kilometers with the signal paths primarily over seawater to minimize propagation effects. Such measurements are reported by *Weidman and Krider* [1978], *Cooray and Lundquist* [1982], and *Murray et al*. [2005]. Similar electric and magnetic field measurements of natural first strokes are reported by *Jerauld et al*. [2008] for 18 natural lightning discharges that terminated within or near the ICLRT measurement network. The measurements described in *Jerauld et al*. [2008] were recorded at distances of less than 1 km over land. The above measurements demonstrated a common sequence of waveform characteristics within 10 μs of the return stroke. This sequence of processes has been generally characterized as the "slow front" and "fast transition." *Weidman and Krider* [1978], who measured electric field waveforms over some tens of kilometers of seawater, noted that the electric field demonstrated a gradual rise prior to the return stroke with typical duration of 1 μs to 8 μs (mean of about 4 μs) followed by a fast rise to peak with duration of 200 ns or less. The gradual rise (the slow front) typically reached amplitude 40% to 50% of the electric field peak due to the following return stroke. *Weidman and Krider* [1978] reported similar electric field measurements of the slow-front and fast-transition sequence for subsequent strokes initiated by dart and dart-stepped leaders. For strokes initiated by dart leaders, they found that the slow front had shorter duration (typically 600 ns to 900 ns) and rose to an average value of about 20% of the return stroke electric field peak. Strokes preceded by dart-stepped leaders were found to exhibit typical slow-front durations of about 2.1 μs with peak amplitude ratios comparable to first strokes. The fast-transition amplitudes for first and subsequent strokes were found to be similar. Similar slow-front and fast-transition sequences have also been observed in the measured current waveforms of direct lightning strikes to tall towers [e.g., *Berger et al*., 1975; *Eriksson*, 1978; *Visacro et al*., 2004].

The physical mechanism that radiates the observed slow-front process in natural first and subsequent strokes has long been a topic of discussion among researchers. An original hypothesis proposed by *Berger and Vogelsanger* [1969] suggested that the slow front for lightning discharges to tall towers was a result of the

UCPL initiated in response to the downward negative leader. Their hypothesis was derived from the observation that natural positive lightning strikes to tall towers often demonstrated long duration, gradually rising current that was correlated in time with optical observations of long upward propagating leaders. *Weidman and Krider* [1978] tested the theory of *Berger and Vogelsanger* [1969] by using a single-wave transmission-line (TL) model [e.g., *Uman and McLain*, 1969] to show that a single upward propagating leader could not accurately reproduce the slow-front amplitude in relation to the subsequent electric field peak. The single-wave TL model predicts the radiated electromagnetic fields by injecting a propagating current wave into the bottom of a channel with the assumption that the current wave propagates upward without attenuation or distortion. The electromagnetic fields are calculated assuming propagation over perfectly conducting ground. As input to the TL model, *Weidman and Krider* [1978] used a current wave with both exponentially increasing amplitude and velocity as a function of altitude (both functions having the same time constant). With reasonable upward leader lengths (constrained to 30 m) and final current amplitudes (constrained to 10 kA), *Weidman and Krider* [1978] calculated electric fields that were similar in waveshape to the measured quantities, but with peaks that were typically much smaller than the measured 5 V/m to 7 V/m field peaks (normalized to 100 km). As a physically plausible alternative, they hypothesized that the slow front could be the result of multiple simultaneously propagating upward positive leaders. Additional attempts to model the slow-front process have been conducted by *Thottappillil and Uman* [1993] and *Cooray et al*. [2004].

The attachment process of triggered lightning return strokes at the ICLRT has been studied by *Jerauld et al*. [2007] and *Howard et al*. [2010]. *Jerauld et al*. [2007], based on the unsuccessful results of previous researchers to model the slow front with a single-wave TL model, extended the approach to utilize a two-wave TL model, in which the current wave injection point was elevated above ground. *Jerauld et al*. [2007] used a measured triggered lightning channel-base current waveform as input to the model. The current waveform was recorded during the third return stroke of a triggered flash that demonstrated a slow-front and fast-transition sequence similar to those observed in association with natural first strokes. Electric and magnetic field waveforms were recorded for the event at distances from the termination point of 15 m and 30 m. *Jerauld et al*. [2007] describe the slow front as being radiated by a pair of microsecond time scale current waves initiated from the elevated junction point that propagate simultaneously away from the junction point as the downward propagating, stepped leader and the UCPL meet. The bidirectional current waves each have amplitude on the order of some tens of kiloamperes. *Jerauld et al*. [2007] describe the fast transition as being radiated by the same bidirectional current wave that establishes the full connection between the stepped leader and the UCPL. The measured field change waveforms at 15 m and 30 m were well reproduced using a downward propagating wave speed of 1.55×10^8 m/s and an upward propagating wave speed of 0.95×10^8 m/s. From video records that showed multiple loops in the channel above the strike object, the junction point was determined to be at an altitude of 6.5 m. The results obtained by *Jerauld et al*. [2007] can also be extended to subsequent strokes, which as stated previously, exhibit slow-front durations that are shorter than those radiated by first strokes (difference of about a factor of five) and smaller slow-front peak amplitude ratios that those radiated by first strokes (difference of about a factor of 2). Considering the sources of the slow front is the charges on the descending negative and ascending positive leaders, and that typical subsequent leaders have about a factor of 5 lower line charge density than do stepped leaders, it is not surprising that subsequent strokes have shorter duration slow fronts with smaller peak amplitude ratios. Subsequent strokes are associated with shorter upward connecting leaders than first strokes as a result of the lower charge density and faster propagation speed of the descending leader.

Howard et al. [2010] extended the work of *Jerauld et al*. [2007] by analyzing the attachment process using three-dimensional source locations of the electric field derivative (d*E*/d*t*) pulses recorded immediately prior to the return stroke. The source locations were determined via data collected from an eight-station time-of-arrival (TOA) network [e.g., *Howard et al*., 2008]. *Howard et al*. [2010] analyzed the leader and postleader phases of three stepped leaders preceding natural first strokes and one dart-stepped leader preceding a triggered lightning return stroke. For both stepped leaders and the triggered lightning dart-stepped leader, *Howard et al*. [2010] identified pulse characteristics within several microseconds of the return stroke that were different from the preceding leader-step pulses. This sequence of pulses was termed a leader burst and occurred prior to the beginning of the slow-front period in the d*E*/d*t* waveforms. The TOA locations of the leader burst pulses typically descended rapidly (and in at least one case, traversed a large horizontal distance), often at speeds more than order of magnitude faster than the average propagation speed of the

preceding leader. In all events analyzed, *Howard et al*. [2010] also found that the leader burst was a very strong emitter of X-rays. Pulses resembling the leader burst had previously been documented by *Murray et al*. [2005] and *Jerauld et al*. [2007] immediately preceding the beginning of the slow front, although no physical explanation or mechanism is provided in either study. For distant electric field waveforms, *Murray et al*. [2005] found that about 57% (75 out of 131 events) exhibited a leader burst in the interval extending from 4 to 9 μs prior to the fast-transition pulse associated with the return stroke. *Murray et al*. [2005] also identified many pulses in the interval from 1 to 4 μs of the dominant d*E*/d*t* pulse associated with the return stroke that could be related to the leader burst process. *Wang et al*. [2001] documented a low-altitude (about 35 m above ground) pulse of light measured with the ALPS photodiode imaging system that occurred less than 2 μs prior to the onset of the slow front in a negative cloud-to-ground discharge that terminated about 2 km from the measuring station. The electric field pulse radiated by the optically observed feature was also recorded and had risetime of about 500 ns. At the time the pulse of light was recorded, the UCPL had already extended to an altitude of 88 m at an average speed of 1.7×10^6 m/s. The electric field pulse characteristics, the timing of the pulse relative to the initiation of the slow front, and the low altitude of the source suggest that the observed pulse may have been associated with a leader burst process. Hence, the leader burst may emit a distinct optical signature and may also occur following the initiation of the UCPL.

Pulses superimposed on the slow front of the d*E*/d*t* waveforms were also analyzed by *Howard et al*. [2010] using the TOA technique. Slow-front pulses had been previously documented by *Murray et al*. [2005] and *Jerauld et al*. [2007]. Although no physical explanation is given for the slow-front pulses, *Jerauld et al*. [2007] did note that the radiation fields of the slow-front pulses were similar in waveshape yet smaller in amplitude than the subsequent fast-transition pulses and that the mechanisms may, in fact, be quite similar. *Murray et al*. [2005] also found that the distant radiation fields of slow-front pulses in their Type B and Type C events demonstrated strong resemblance to the subsequent fast-transition pulses associated with the return stroke. The analyses of *Howard et al*. [2010] did not refute these prior observations. *Howard et al*. [2010] found that the TOA locations of the slow-front pulses occurred at very low altitude and in the same spatial proximity as the TOA location of the fast-transition pulse, suggesting that the slow-front pulses may be involved in the interaction between the upward and downward leaders (the mechanism by which the slow front is radiated according to the modeling results of *Jerauld et al*. [2007]) prior to the full connection being established. *Howard et al*. [2010] suggested that there may be no physical difference between the slow front and fast-transition pulses and that the defining characteristic is simply emission time. This view is supported by an observation reported by *Howard et al*. [2010] for a slow-front pulse preceding a rocket-triggered lightning return stroke that occurred when the channel-base current had risen to a level of 20 kA. This current amplitude is uncharacteristic of a UCPL current and indicates that a connection between the descending dart-stepped leader and upward connecting leader already existed.

Wang et al. [2013] analyzed the attachment process of five triggered lightning dart-stepped leaders at the ICLRT using the LAPOS (Lightning Attachment Process Observation System) high-speed optical imaging system. *Wang et al*. [2013] resolved bidirectional current wave propagation associated with the attachment process for three of the dart-stepped leaders. The reported downward current wave propagation speeds ranged from 7.0×10^7 m/s to 1.9×10^8 m/s. The return stroke initiation heights above the strike object estimated by *Wang et al*. [2013] for the five dart-stepped leaders ranged from 9.7 m (±2.4 m) to 21 m (±4.6 m).

The prior studies summarized here have identified commonly occurring electromagnetic characteristics of the attachment process with some plausible physical explanations. In the present study, an extensive data set of time-correlated electromagnetic fields, sensitive channel-base currents, and high-speed/high-definition video records is used to further refine the sequence of events that comprise the attachment process for triggered lightning strokes, and more importantly, establish the physical significance of the observed leader burst, slow-front pulse, and fast-transition processes. The data presented were recorded during the summers of 2013 and 2014 at the ICLRT.

2. Experimental Setup

In Figure 1, an aerial photograph is shown with annotated locations of the ICLRT rocket-launching facility, d*E*/d*t* sensors, and the high-speed/high-definition video cameras. High-speed video images were recording using a Vision Research Phantom v711 camera. During 2013, the camera was located 292 m northwest of the launching

Figure 1. Aerial photograph of the ICLRT showing the locations of the d*E*/d*t* measurement stations, the high-speed camera locations, and the launching facility.

facility. The camera was equipped with a 20 mm Canon lens set to an aperture of f/2.8. In 2014, the camera was located 205 m to the northeast of the launching facility and was equipped with a Canon 10–22 mm lens set to an aperture of f/3.8. The resolution of the camera during both summers was set to 208 × 24 pixels providing a vertically-oriented field of view of about 60 m × 7 m. The spatial resolution was about 0.3 m/pixel. The camera was set to record in 12-bit gray scale resolution at a frame rate of 647,619 frames per second, providing an exposure time of 1.16 μs and a dead-time of 380 ns, for a total frame time of 1.54 μs. The exposure of the camera was configured to resolve dimmer optical features of the leader step formation and attachment processes, while necessarily saturating on the brighter portions of the leader and return stroke optical signatures. Video frames presented in this paper have been inverted and contrast enhanced to better illustrate the relevant optical features of the attachment process. *Gamerota et al.* [2014b] have previously documented the leader step formation process of three dart-stepped leaders recorded during 2013 using the high-speed video setup described above. The images shown in Figure 2 and Figure 3 of *Gamerota et al.* [2014b] are reproduced in this paper on different spatial scales in Figures 2a and 5, respectively. Supplementary high-definition video images of the triggered lightning channel were recorded at distances of 155 m and 21 m from the launching facility using Canon HFS-21 high-definition video cameras operating at 30 frames per second.

Triggered lightning leaders attached to a 1.6 m strike rod bonded to the metallic launcher. The top of the strike rod was located at an altitude of about 5.7 m (Figure 2b). The channel-base current was sensed by a 1 mΩ current shunt (T&M Research model R-7000-10) with bandwidth of 8 MHz. The shunt was mounted in a large stainless steel enclosure beneath the metallic launcher (Figure 2b). The shortest current path length between the top of the strike rod and the shunt was about 5 m. The output of the shunt was carried over a 0.5 m length of coaxial cable to a pair of HBM 7600 Isolated Digitizers. The dynamic ranges of the digitizers were configured to record current levels up to 50 kA and 500 A, respectively. The more sensitive current measurement had resolution of about 1 A. After passing through the shunt, the channel-base current was routed over a 1 m length of braided wire to a network of three vertical 13 m ground rods connected in parallel with triangular spacing of about 0.1 m. The braided wire passed through the aperture of a Prodyn RID-250A I-dot coil, which sensed the first derivative of the channel-base current. The I-dot coil has bandwidth greater than 300 MHz. The output of the I-dot coil was passed through a 30 dB attenuator and was then routed to a HBM 7600 Isolated Digitizer.

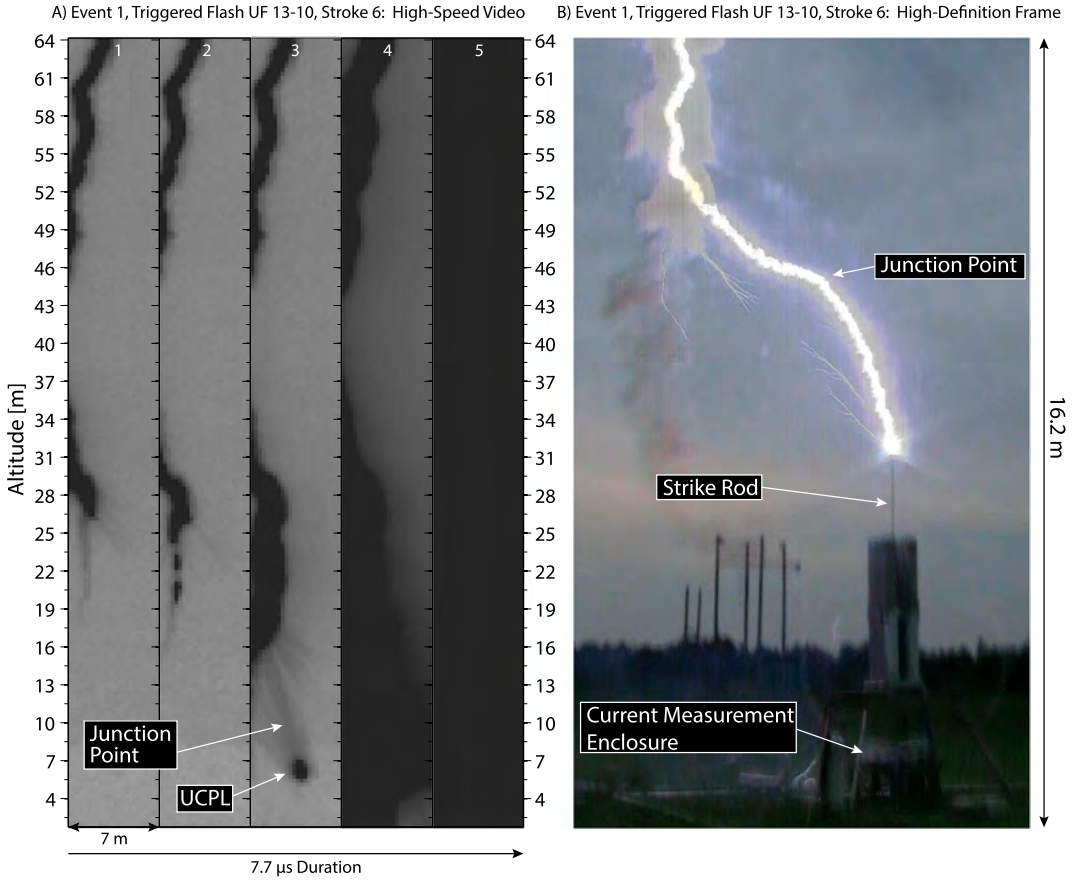

Figure 2. (a) Five consecutive 1.54 μs frames (7.7 μs total duration) showing the final downward leader step (Frames 1–3) and the subsequent attachment process (Frames 3–4) for the sixth return stroke of triggered flash UF 13–10 on 14 June 2013, Event 1. (b) Cropped high-definition video frame (30 ms exposure) recorded a distance of 21 m from the launching facility showing the attachment of the upward and downward leaders. Multiple unconnected upward and downward leaders are imaged in Figure 2b. Note the vertical scales in Figures 2a and 2b are different by a factor of four. The junction point between the UCPL and downward leader is annotated in Figures 2a and 2b.

During 2013, a network of 10 flat-plate d*E*/d*t* sensors were arrayed about the launching facility. The sensors were configured to operate as a TOA network optimized for locating low-altitude d*E*/d*t* sources in three dimensions with a high degree of spatial and temporal accuracy [e.g., *Hill et al*., 2012]. The outputs of all sensors were connected to equals lengths of RG223U coaxial cable and were digitized using HBM 7600 Isolated Digitizers housed in stainless steel enclosures. In order to well resolve all leader-step field changes, nine of the sensors were configured to record narrow dynamic ranges of about ±7.25 kV/m/μs. One sensor, dE-25, located 142 m from the launching facility, was configured to record a large dynamic range to resolve the return stroke field change. During 2014, an additional sensor (dE-50) was added about 51 m south of the launching facility. The original 10 sensors were all configured to record leader step field changes, while dE-50 was configured to record the return stroke field change. The increased sensitivity of the d*E*/d*t* TOA network relative to the system used by *Howard et al*. [2010] provided greatly increased amplitude resolution for lower-amplitude field changes during the leader phase and the initial portion of the attachment process. The adverse effect of the narrower dynamic range was that large-amplitude pulses during the attachment process (e.g., slow-front pulses and fast-transition pulses) often saturated the closer sensors, rendering the accurate three-dimensional TOA calculations of these sources more difficult.

All HBM 7600 Isolated Digitizers operated at a sampling rate of 100 MS/s with 14-bit amplitude resolution. The analog bandwidth of the digitizer front end is 25 MHz. Additionally, all signals were low-pass filtered at the digitizer front end with L-Com BLP 21.4+ antialiasing filters. The digital data were transmitted over single-mode fiber optic cables to a HBM Gen16t Transient Recorder located in the main office building. The HBM

Table 1. General Information on the Three Triggered Lightning Dart Stepped Leader/Return Stroke Sequences

Event	Flash	Date	Time (UTC)	Stroke Order	Return Stroke Peak Current (kA)
1	UF 13–10	14/06/2013	20:59:31.030563	6	14.7
2	UF 13–10	14/06/2013	20:59:31.203258	8	12.3
3	UF 14–27	14/07/2014	19:14:59.767952	6	13.7

Gen16t Transient Recorder automatically calculated and removed fiber-optic propagation delays to each attached digitizer each time data were acquired with accuracy of 10 ns. The data acquisition system and high-speed camera were triggered to record when the channel-base current surpassed a predefined threshold of about 5 kA. Waveform data were recorded in 30 ms segments with 15 ms of pretrigger.

3. Data and Analysis

Three data sets including recorded current, d*I*/d*t*, and d*E*/d*t* waveforms, and high-speed video images are presented as examples of the attachment process of triggered lightning dart-stepped leaders. General parameters of the three leader/return stroke sequences are given in Table 1. The three leader events are associated with subsequent return strokes with typical triggered lightning peak currents of 12–15 kA [e.g., *Rakov and Uman*, 2003]. For convenient reference throughout this paper, the sixth stroke of flash UF 13–10, the eighth stroke of flash UF 13–10, and the sixth stroke of flash UF 14–27 will be henceforth referred to as Event 1, Event 2, and Event 3, respectively. These particular data were selected primarily based on the content of the high-speed video images. In order to clearly delineate the electromagnetic and optical features that comprise the attachment process, it is very helpful if the attachment process is imaged in consecutive 1.54 μs frames. In some cases, the entire attachment process is imaged in a single frame, and thus, the lower luminosity features of the early stages of the attachment are masked by the much brighter subsequent stage.

Three figures are shown for Event 1, Event 2, and Event 3 in chronological order: (1) consecutive 1.54 μs high-speed video images extending from the microseconds immediately prior to the attachment process through the return stroke (Figures 2, 5, and 8), (2) low-amplitude d*E*/d*t* and channel-base current waveforms plotted on a 30 μs time scale (Figures 3, 6, and 9), (3) short time scale (<5 μs) d*E*/d*t* waveforms plotted with high-amplitude current and d*I*/d*t* (Figures 4, 7, and 10). All low-amplitude d*E*/d*t* waveforms were measured 225 m from the channel at Station 7 (Figure 1). The time periods corresponding to the high-speed video images in Figures 2, 5, and 8 are annotated in Figures 3, 6, and 9. High-amplitude d*E*/d*t* waveforms were

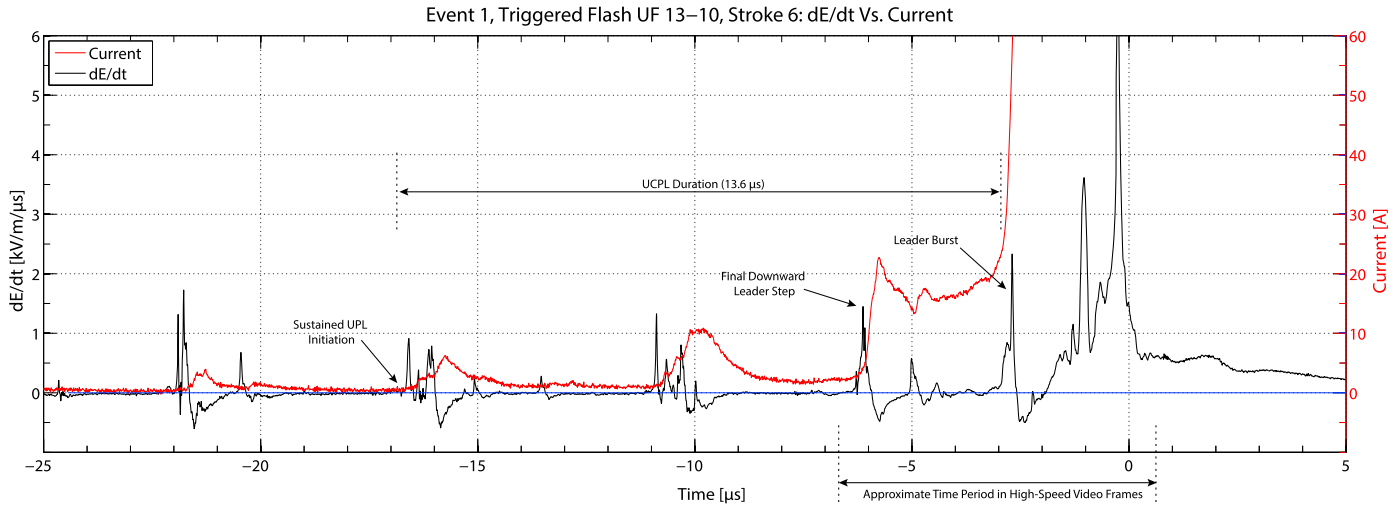

Figure 3. Thirty-microsecond d*E*/d*t* (black) and channel-base current (red) for the sixth return stroke of triggered flash UF 13–10 on 14 June 2013, Event 1. The peak of the return stroke current corresponds to time zero. The UPL initiation, UPL duration, final downward leader step, and leader burst processes are annotated in addition to the corresponding time window displayed by the high-speed video frames in Figure 2. The electromagnetic wave propagation delay between the launcher and the d*E*/d*t* measurement station has been removed from the d*E*/d*t* waveform.

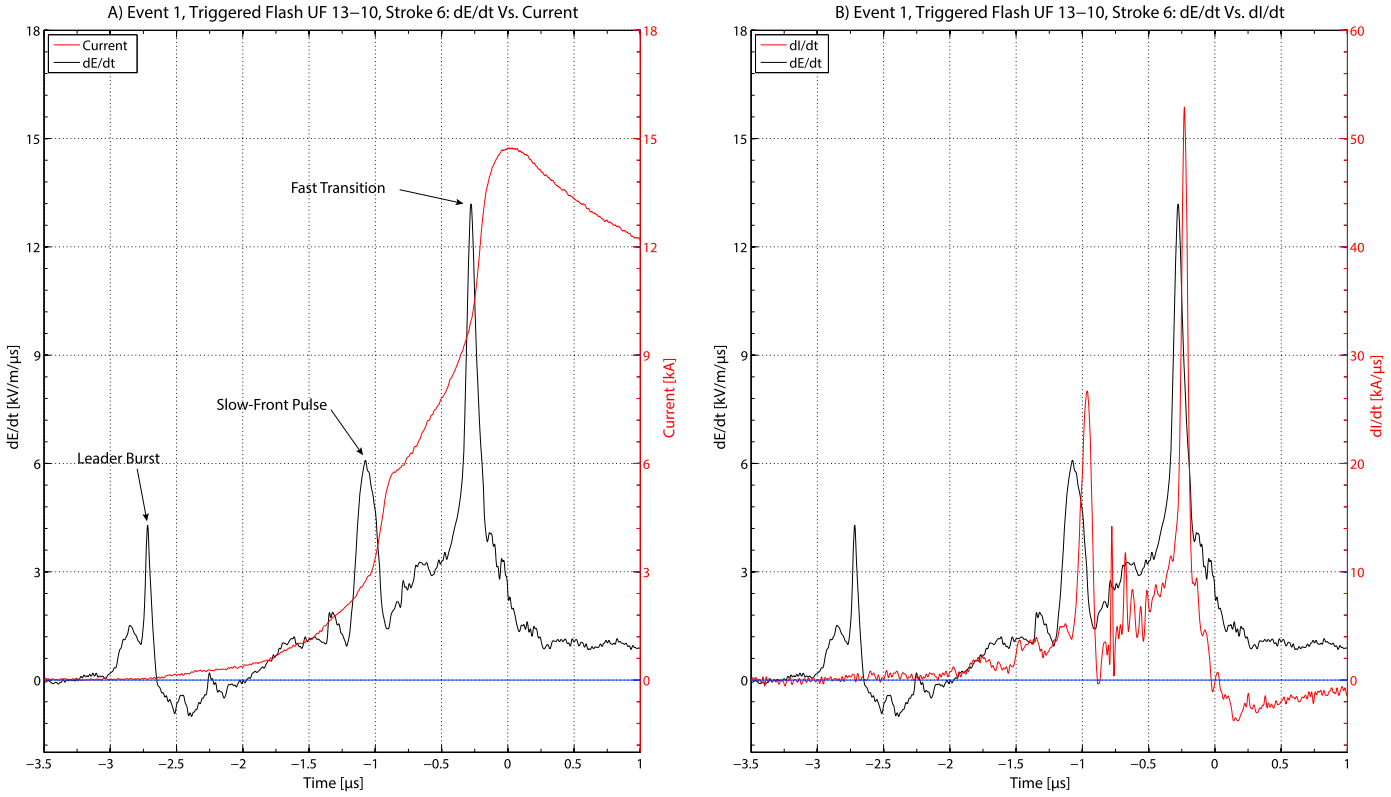

Figure 4. (a) Channel-base current (red) records and 4.5 µs d*E*/d*t* (black) for the sixth return stroke of trigged flash UF 13–10 on 14 June 2013, Event 1. The leader burst, slow-front pulse, and fast-transition pulse are annotated. (b) d*I*/d*t* (red) records and 4.5 µs d*E*/d*t* (black) showing the time delays between the d*E*/d*t* and d*I*/d*t* peaks for the slow-front and fast-transition pulses. The electromagnetic wave propagation delays between the launcher and the d*E*/d*t* measurement station have been removed from the d*E*/d*t* waveforms.

measured at Station 25 during 2013 and Station 50 during 2014. In all waveform plots, the electromagnetic wave propagation delay has been removed between the launcher and the respective d*E*/d*t* sensor location in order to align the d*E*/d*t* and current waveforms. The only remaining time delay (to be measured) is associated with the propagation of the current from some height in the channel to the current measuring sensors. Time zero in the waveform plots corresponds to the peak of the return stroke current. d*E*/d*t* waveforms and vertical scales are shown in black and current waveforms and vertical scales are shown in red.

The sequence of electromagnetic and optical features that comprise the attachment process will be analyzed in order of time of occurrence relative to the return stroke in sections 3.1. Data from all three leader/return stroke sequences will be considered in the analysis of each feature.

3.1. Initiation of the Sustained UCPL

Beginning several tens of microseconds prior to the attachment of the descending dart-stepped leader to ground, transient current pulses with typical widths of 1–2 µs were measured on the metallic launching structure. The polarities of the current pulses are indicative of positive charge flowing upward through the current measuring device. For Event 1, an example is shown in Figure 3 at −22 µs. The dart-stepped leader step at −22 µs produced a 5 A current pulse measured at ground level. The current slowly decayed back to the system noise level over the next 4.5 µs (recall that the vertical resolution of the current measurement is about 1 A). Similar examples are shown for Event 3 (Figure 9) for d*E*/d*t* leader step field changes occurring at −19 µs, −17.5 µs, −14.5 µs, and −11.5 µs. The amplitudes of the associated current pulses range from 1 A to 3 A. For all cases, the peaks of the current pulses occur in time following the leader step radiation field peaks.

As the descending leader approaches ground, the current measured at ground level in response to downward leader steps ceases to return to the system noise level during the subsequent interstep interval. For Events 1 (Figure 3), 2 (Figure 6), and 3 (Figure 9), this occurs coincident with the leader steps at −16.5 µs,

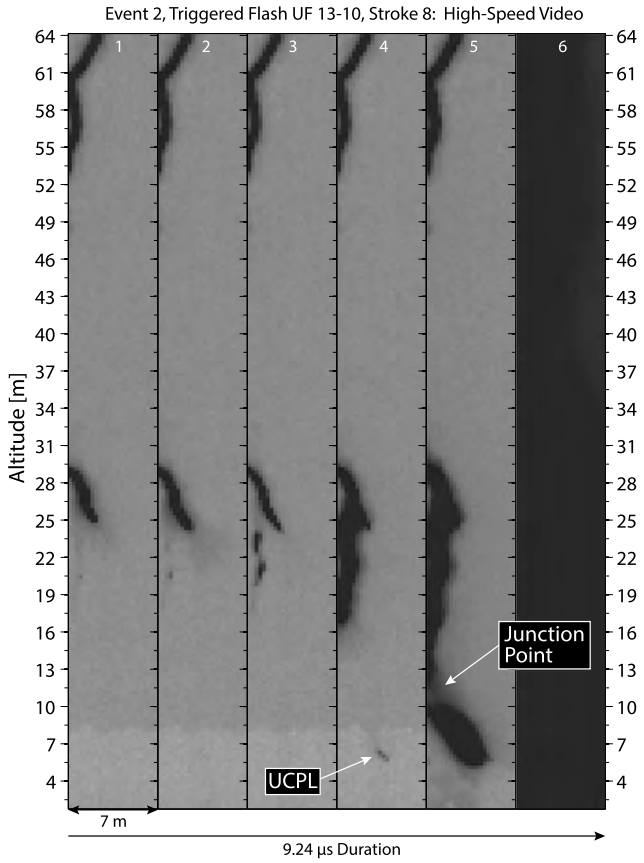

Figure 5. Six consecutive 1.54 µs frames (9.24 µs total duration) showing the final downward leader step and the subsequent attachment process for the eighth return stroke of triggered flash UF 13–10 on 14 June 2013, Event 2.

−24.5 µs, and −9.5 µs, respectively. The beginning of this background current flow is interpreted here as the initiation of the sustained UCPL (see section 4 for additional details). Following the initiation of the UCPL, the background current level between the transient current pulses associated with each leader step tends to gradually increase. The amplitudes of the transient current pulses superimposed on the background current also increase as the descending leader approaches ground.

3.2. Leader Burst

For Event 1, the final downward leader step occurs at −6.5 µs in Figure 3. The formation of the final leader step of Event 1 is shown in the high-speed video images of Figure 2a in Frames 1–3. In Frame 1, the bright leader tip is at 26.5 m altitude with a streamer zone extending downward another 9 m. In Frame 2, two space leaders associated with the leader step formation at −6.5 µs occur within the streamer zone of the prior frame [e.g., *Gamerota et al.*, 2014b]. There is no detectable luminosity associated with the UCPL in Frame 2. In Frame 3, the bidirectional propagating space leaders connect with the leader channel above, and the new

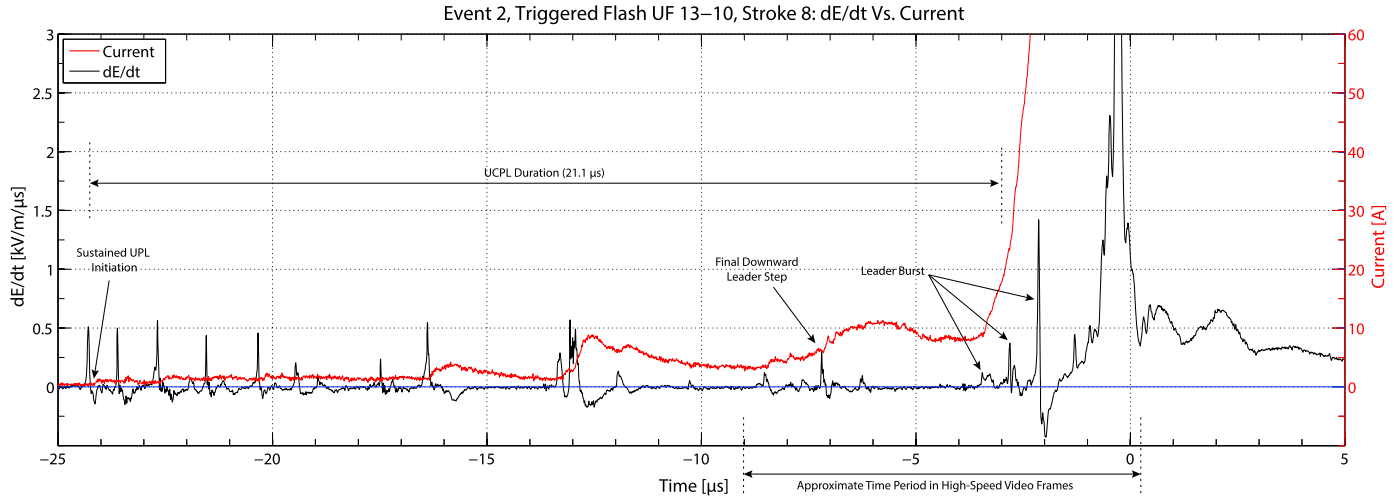

Figure 6. d*E*/d*t* (black) and channel-base current (red) for the eighth return stroke of triggered flash UF 13–10 on 14 June 2013, Event 2. The peak of the return stroke current corresponds to time zero. The UPL initiation, UPL duration, final downward leader step, and leader burst processes are annotated in addition to the corresponding time window displayed by the high-speed video frames in Figure 5. The electromagnetic wave propagation delay between the launcher and the d*E*/d*t* measurement station has been removed from the d*E*/d*t* waveform.

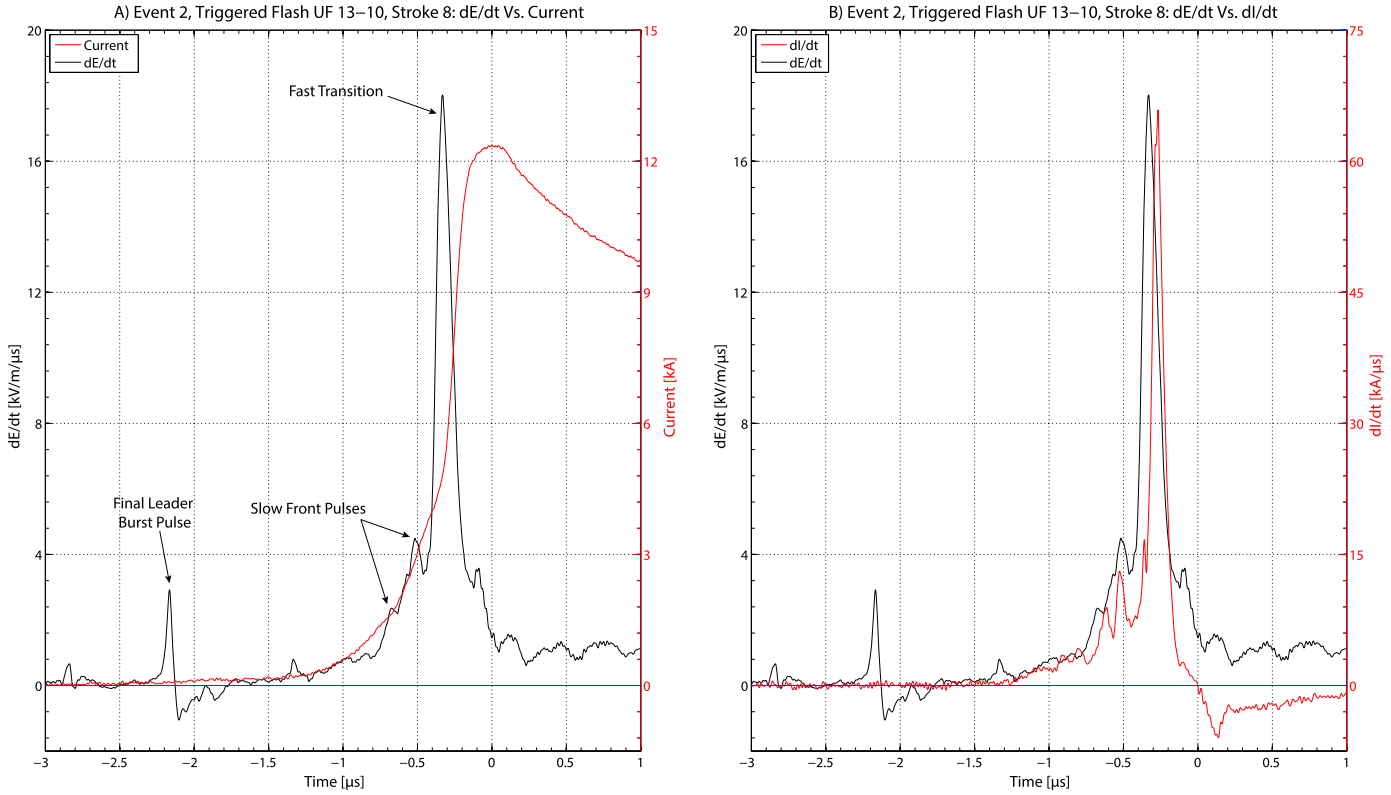

Figure 7. (a) Four microsecond d*E*/d*t* (black) and channel-base current (red) records for the eighth return stroke of trigged flash UF 13–10 on 14 June 2013, Event 2. The leader burst, slow-front pulses, and fast-transition pulse are annotated. (b) Four microsecond d*E*/d*t* (black) and d*I*/d*t* (red) records showing the time delays between the d*E*/d*t* and d*I*/d*t* peaks for the slow-front and fast-transition pulses. The electromagnetic wave propagation delays between the launcher and the d*E*/d*t* measurement station have been removed from the d*E*/d*t* waveforms.

section of leader channel progresses downward. The TOA location of the d*E*/d*t* pulse peak of the final leader step was at 25 m altitude with vertical error on the order of 1 m, near the connection point between the bidirectional leader and the leader channel above. Frame 3 also shows a 1.5 m UCPL propagating from the tip of the strike rod located at 5.7 m altitude. The streamer zones of the UCPL and downward leaders are shown overlapping with the tips of the leaders separated by about 7 m. In Figure 3, a 23 A current pulse was measured following the final downward leader step at −6.5 µs, after which the background current decayed to an average value of about 16 A for the next several microseconds. The optical blooming in Frame 3 is increased relative to Frame 1 and Frame 2, a characteristic likely associated with the small background current flow due to the initial interaction of the upward and downward streamer zones. At −3 µs in Figure 3, the current rises sharply coincident with a large d*E*/d*t* pulse that occurs immediately prior to the beginning of the d*E*/d*t* slow front. Unlike the earlier current pulses associated with leader step field changes, this sharp current increase was not delayed relative to the d*E*/d*t* peak. That d*E*/d*t* pulse is classified as the leader burst in Figure 3. *Murray et al*. [2005], *Jerauld et al*. [2007], and *Howard et al*. [2010] reported that the leader burst was typically composed of multiple d*E*/d*t* pulses in succession, although in this case, the leader burst appears to have been a single, large-amplitude pulse. The d*E*/d*t* TOA location of the leader burst pulse peak was at 17.5 m with 1 m of vertical uncertainty in the computed solution, placing it near the tip of the downward leader in Frame 3 of Figure 2a. A single, high-definition video frame of the connection region between the downward and upward leaders is shown in Figure 2b. Based on the ending locations in space of the unconnected downward and upward leaders shown in Figure 2b, the junction point between the downward and upward leaders is estimated to have occurred at the kink in the channel located 3.5 m above the tip of the strike rod at an altitude of about 9.5 m. The leader burst pulse was located 8 m above the junction height.

The final downward leader step of Event 2 occurred at −7 µs in Figure 6. The step formation is shown in Frames 1–3 of Figure 5. Two space stems formed below the leader channel tip in Frame 1, then transitioned to bidirectionally propagating space leaders in Frame 2 and Frame 3. No luminosity associated with a UCPL is

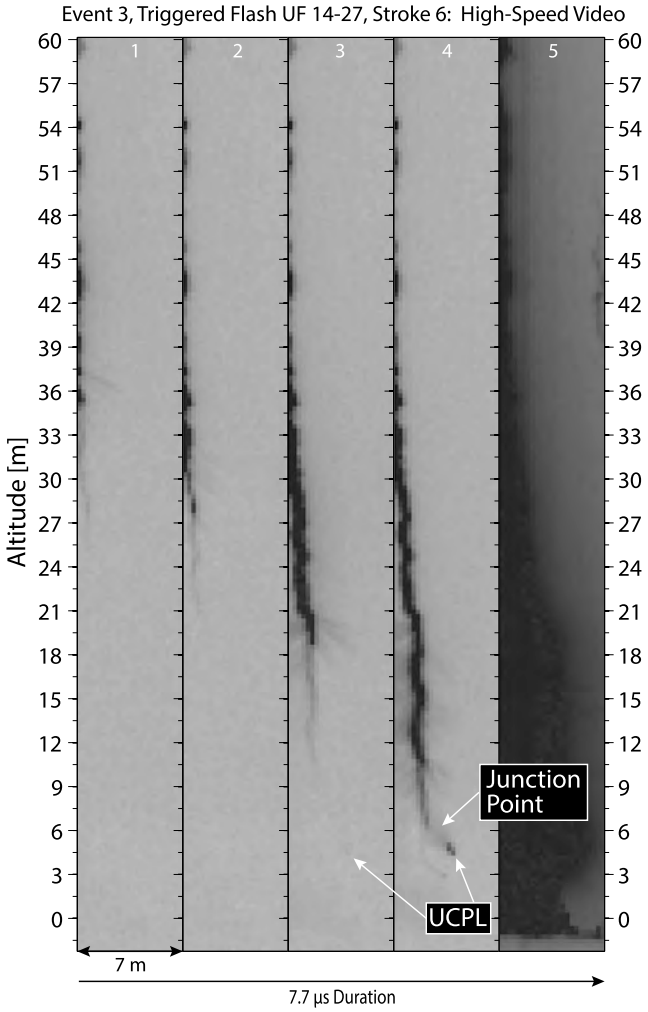

Figure 8. Five consecutive 1.54 μs frames (7.7 μs total duration) showing the final three downward leader steps and the subsequent attachment process for the sixth return stroke of triggered flash UF 14–27 on 14 July 2014, Event 3.

visible in Frame 3. The new leader step formed in Frame 4, with the tip located at an altitude of about 16 m. An UCPL with length of about 1.5 m is also shown in Frame 4 originating from the tip of the strike rod. Similar to Event 1, the TOA location of the dominant d*E*/d*t* pulse peak associated with the final leader step was located at about 25 m, near the connection point of the bidirectional space leaders and the prior leader channel tip above. In Figure 6, the current increased to about 11 A following the final leader step, and then slowly decayed to a level of 9 A for a time period of about 1.5 μs. The first leader burst pulse was recorded at −3.5 μs, followed by two, larger amplitude pulses over the next 1.5 μs. The current increased to about 20 A with the first leader burst pulse, again without the delay measured with the leader step pulses, and then rose sharply with the latter two leader burst pulses. Frame 5 in Figure 5 shows the optical progression of the UCPL during the leader burst process. The UCPL extended to a length of about 6.3 m with a clear streamer zone area between the downward leader tip and the UCPL. The optical blooming of the channel is indicative of the increased background current flow shown in Figure 6. The TOA altitudes of the three leader burst pulse peaks were 18 m, 11 m, and 21 m, respectively, with vertical uncertainties on the order of 1 m in each case. The second leader burst pulse peak, which was time coincident with the initial fast rise of the channel-base current, was TOA located near the apparent connection point of the downward and upward leaders at an altitude of about 11 m. The first and third leader burst pulse peaks were TOA located above the junction point by 7–10 m. The multipulse leader burst shown in Figure 6 is more representative of the leader burst events previously documented in the literature.

The high-speed video shown in Figure 8 for Event 3 encompasses the final three downward leader steps. The third to last leader step occurred at −7 μs in Figure 9 and is shown in Frame 1 of Figure 8. The TOA altitude of the dominant leader step d*E*/d*t* pulse peak was at 42.5 m (about 1 m of vertical uncertainty), which is located nearly exactly at the lowest point in space of the prior leader step (not shown in Figure 8). A 6.5 A current pulse was recorded in response to the second to last leader step, after which the current decayed to a level of about 5 A. The second to last downward leader step at −5.5 μs is shown in Frame 2 of Figure 8. The TOA altitude of the dominant leader step d*E*/d*t* pulse peak was at 30 m, several meters below the location of the leader tip from the prior step. The current rose to about 7 A following the leader step, and then decayed over a microsecond to 6 A. The final leader step occurred at −3.5 μs and is shown in Frame 3 of Figure 8. The TOA altitude of the final step was at about 28 m, again coinciding with the lowest point in space of the bright leader tip associated with the prior step. The downward streamer zone of the final step extended below the bright leader tip another 9 m to an altitude of about 10.5 m. A faint but visible UCPL is shown originating from

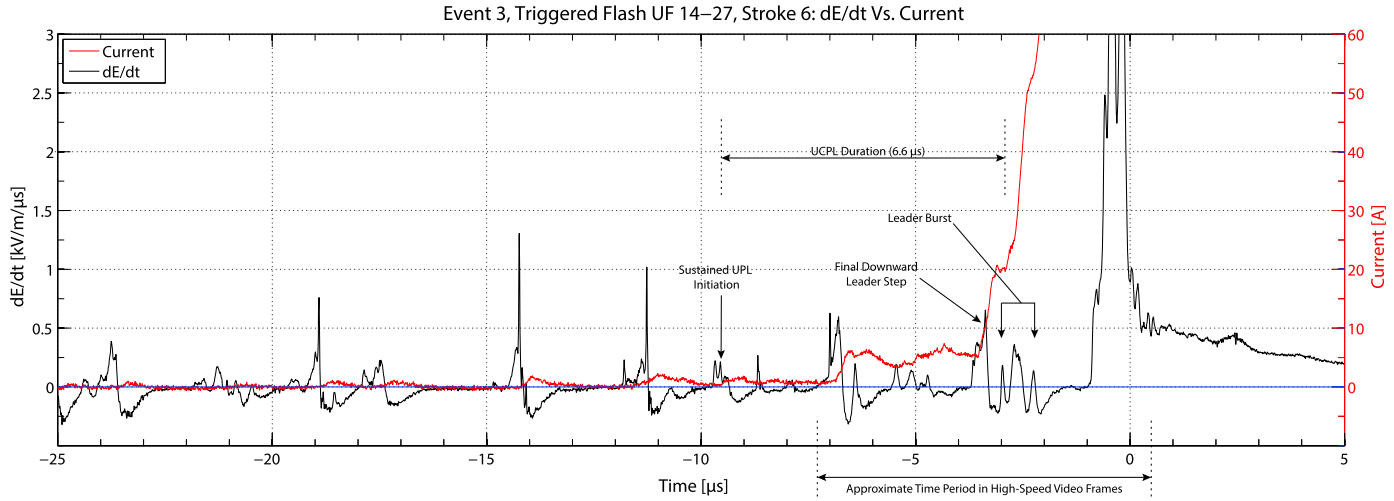

Figure 9. d*E*/d*t* (black) and channel-base current (red) for the sixth return stroke of triggered flash UF 14–27 on 14 July 2014, Event 3. The peak of the return stroke current corresponds to time zero. The UPL initiation, UPL duration, final downward leader step, and leader burst processes are annotated in addition to the corresponding time window displayed by the high-speed video frames in Figure 8. The electromagnetic wave propagation delay between the launcher and the d*E*/d*t* measurement station has been removed from the d*E*/d*t* waveform.

the tip of the strike rod in Frame 3. The channel-base current increased to 20 A following the final leader step, then leveled off for several hundred nanoseconds. The first of three leader burst pulses was recorded at −3 μs in Figure 9. Similar to Event 1 and Event 2, the channel-base current rose sharply time coincident with the leader burst pulses. The TOA altitudes of the three leader burst pulse peaks were about 23.5 m, 15 m, and 17.5 m, respectively, all with vertical uncertainties on the order of 1 m. Frame 4 of Figure 8 captured the optical interactions of the upward and downward leaders during the leader burst process. Frame 4 shows a bright UCPL propagating from the strike rod with length of about 1 m. The UCPL is separated from the brighter tip of the downward leader by less than 2 m. There is also a second, dimmer channel in Frame 4 that connects the tip of the downward leader to the rocket tubes located 1.7 m below the tip of the strike rod. In this case, the TOA locations of the leader burst pulse peaks were all above the connection region of the downward and upward leaders, which from Figure 8, appears to have occurred at an altitude of about 6 m.

3.3. Slow Front and Fast Transition

The d*E*/d*t* slow front begins immediately following the single leader burst pulse in Event 1 at about −2.5 μs in Figure 3. A d*E*/d*t* record is overlaid on the high-level channel-base current in Figure 4a and on the d*I*/d*t* waveform in Figure 4b. Following the leader burst pulse, which established the initial connection between the upward and downward leaders, the channel base increased rapidly over the next 2.5 μs to an amplitude of 3 kA. Then, the current increased to about 5.7 kA coincident with a single, larg- amplitude d*E*/d*t* pulse. This pulse superimposed on the d*E*/d*t* slow front is similar to the slow-front pulses documented by *Jerauld et al*. [2007] and *Howard et al*. [2010]. As expected, there is a large d*I*/d*t* pulse with amplitude of about 26 kA/μs in Figure 4b associated with the fast increase in channel-base current from 3 kA to 5.7 kA. More important is the observed delay of 110 ns in Figure 4b between the peak of the d*E*/d*t* slow-front pulse and the related d*I*/d*t* pulse. With the free-space propagation path length delay removed from the d*E*/d*t* time base, the only possible source of delay between the d*E*/d*t* and d*I*/d*t* waveforms occurs because the d*E*/d*t* waveform is radiated from an elevated source. The delay between the d*E*/d*t* and d*I*/d*t* waveforms is representative of the current wave propagation time from the elevated junction point of the upward and downward leaders to the current measurement device located near ground level. The video records of Figure 2 showed that the connection point occurred about 3.5 m above the tip of the strike rod. By accounting for the curvature of the UPL, the total path length between the connection point and the strike rod was about 4 m. The shortest path length between the tip of the strike rod and the current measurement device is about 5 m. Assuming that the current wave propagates at the speed of light within the metallic launching structure, the average speed of the downward propagating current wave between the junction point and the tip of the strike rod can be calculated according to equation (1), where $\text{Dist}_{\text{Junction}}$ is the distance between the junction point

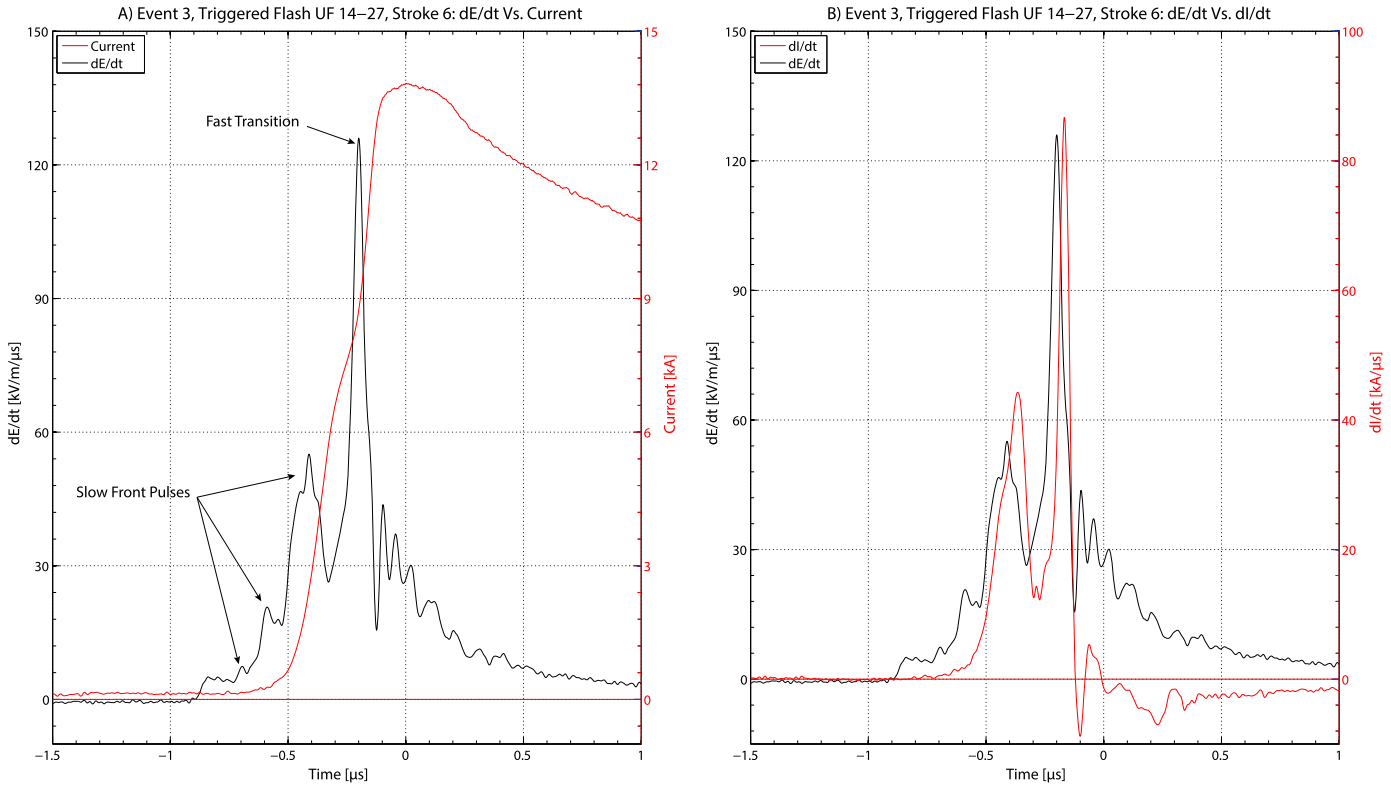

Figure 10. (a) Channel-base current (red) records and 2.5 µs d*E*/d*t* (black) for the sixth return stroke of trigged flash UF 14–27 on 14 July 2014, Event 3. The slow-front pulses and fast-transition pulse are annotated. (b) d*I*/d*t* (red) records and 2.5 µs d*E*/d*t* (black) showing the time delays between the d*E*/d*t* and d*I*/d*t* peaks for the slow-front and fast-transition pulses. The electromagnetic wave propagation delays between the launcher and the d*E*/d*t* measurement station have been removed from the d*E*/d*t* waveforms.

and the strike rod tip, Delay is the measured time delay between the d*E*/d*t* and d*I*/d*t* peaks, and *c* is the speed of light in a vacuum.

$$V_{\text{Downward}} = \frac{\text{Dist}_{\text{Junction}}}{\text{Delay} - \frac{5}{c}} \tag{1}$$

For the slow-front pulse shown in Figure 4, the average downward propagating current wave speed in free space was 4.3×10^7 m/s assuming the current wave associated with the slow-front pulse initiated at the junction point 4 m from the tip of the strike object. Frame 4 of Figure 2 shows the high-speed video associated with the slow-front pulse. A clear channel connection has been established at this point. The frame is not completely saturated due to the moderate current level (5.7 kA). Following the slow-front pulse, the channel-base current rose to 10 kA in a time span of about 550 ns and then elevated sharply to 14 kA coincident with the largest d*E*/d*t* pulse in Figure 4. The largest d*E*/d*t* pulse is referred to as the fast transition in the prior literature and is typically associated with the dominant return stroke field change. For the fast-transition pulse, the delay between the d*E*/d*t* and d*I*/d*t* peaks was 50 ns. Assuming the same junction location 4 m from the tip of the strike object, the downward current wave propagation speed was 1.2×10^8 m/s. The total time duration between the beginning of the attachment, marked in time by the initial fast current rise associated with leader burst pulse, and the peak of the d*I*/d*t* associated with the fast transition, our definition of the attachment process duration, was about 2.7 µs. The optical signature of the fast transition was captured in Frame 5 of Figure 2, which completely saturated the camera sensor.

Similar to Event 1, the d*E*/d*t* slow front for Event 2 initiated immediately following the final leader burst pulse at −2.2 µs in Figure 7a. The current ramped sharply for 1.5 µs to an amplitude of about 1.5 kA. Several small-amplitude d*E*/d*t* slow-front pulses were recorded over the next 200 ns, with two associated d*I*/d*t* peaks. The channel-base current quickly increased to about 4 kA as a result of the slow-front pulses. The delay between the first d*E*/d*t* slow-front pulse at −700 ns and the corresponding d*I*/d*t* peak was 60 ns. The high-speed video

images of Figure 5 show the junction point between the upward and downward leaders located about 7 m from the tip of the strike rod. From equation (1), the calculated downward current wave speed for the first slow-front pulse was 1.6×10^8 m/s, assuming that the current source was initiated 7 m from the tip of the strike object. The timing relationship between the d*E*/d*t* slow-front pulses and the second d*I*/d*t* pulse is ambiguous due to the small hitch in the d*E*/d*t* waveform at −600 ns. After the rapid current increase coincident with the d*E*/d*t* slow-front pulses, the current elevated more slowly in Figure 7a over the next 100 ns, then ascended rapidly to an amplitude of 12 kA with the fast-transition d*E*/d*t* pulse. The delay between the d*E*/d*t* and d*I*/d*t* fast-transition peaks was also 60 ns, giving a downward current wave speed of 1.6×10^8 m/s assuming the current source associated with the fast transition initiated 7 m from the tip of the strike object. The optical signatures of the slow-front and fast-transition pulses were both captured in Frame 5 of Figure 5, completely saturating the camera sensor.

In Event 3, the beginning of the d*E*/d*t* slow front was delayed from the final leader burst pulse by more than 1 μs (Figure 9). During this time period, the channel-base current increased slowly to several hundred amperes. At −700 ns in Figure 10a, the channel-base current began to increase rapidly coincident with several small d*E*/d*t* slow-front pulses. The first two slow-front pulses in Figure 10a were not accompanied by pronounced d*I*/d*t* pulses. The current ascended rapidly with the large d*E*/d*t* slow-front pulse at -400 ns, reaching an amplitude of about 7 kA. The time delay between the large d*E*/d*t* slow-front pulse and the associated d*I*/d*t* pulse in Figure 10b was 44 ns. From the high-speed video images shown in Figure 8, the junction point between the upward and downward leaders was located only about 2 m from the tip of the strike rod, providing a calculated downward current wave speed of 7.3×10^7 m/s. The d*E*/d*t* fast-transition pulse was recorded about 200 ns following the large slow-front pulse. The channel-base current increased to nearly 14 kA with the fast-transition pulse. The fast-transition d*E*/d*t* and d*I*/d*t* peaks were delayed by only 32 ns. The resultant downward current wave propagation speed was 1.3×10^8 m/s assuming a junction point located 2 m from the tip of the strike object. The optical signature of the large slow-front and fast-transition pulses were captured in Frame 5 of Figure 8. Interestingly, no connection was imaged following the faintly luminous path between the bottom of the downward leader channel and the rocket tubes below the strike rod shown in Frame 4.

4. Discussion

For the three dart-stepped leader events presented in section 3, sensitive channel-base current records indicated that the sustained UCPLs were initiated 16.5 μs, 24.5 μs, and 9.5 μs prior to the return stroke current peaks, and 13.6 μs, 21.1 μs, and 6.6 μs prior to the initial large increases in channel-base current time-coincident with the leader burst pulses. Interestingly, in each case, the optical signatures of the UCPLs were not visible in the high-speed video until two frames prior to the frame containing the fast transition, a time period of no more than 3.08 μs. This observation suggests that UCPLs develop both slowly and with minimal luminosity in response to leaders preceding subsequent strokes. It is possible that the observed low-amplitude background current flow observed up to 24.5 μs prior to the return stroke peak is initially the result of multiple, dim corona discharges emanating from the launching structure that eventually transition to a thermalized leader channel a few microseconds prior to the return stroke. Lingering rocket exhaust may also affect the ability of the camera to resolve the dim initial portion of the UCPL. It is also possible that in addition to conduction current, displacement current associated with the increasing electric flux density above the launcher as the negative leader charge descends contributes to the measured current attributed to the UCPL in Figures 3, 6, and 9. The UCPLs became more brightly illuminated in the microseconds immediately prior to the attachment when the descending leader channels were within a short distance of the strike object, less than 15 m in each of the three cases described in section 3. From the high-speed and high-definition video images shown in Figures 2, 5, and 8, the final lengths of the three UCPLs shown in section 3 were 4 m, 7 m, and 2 m. Considering the spatial and temporal resolution of the video images, the final UCPL lengths are expected to be accurate to within 1 m. These UCPL lengths are shorter than the 8 m to 22 m UCPLs reported by *Biagi et al*. [2009], possibly due to differences in the launcher configuration. The data recorded by *Biagi et al*. [2009] were associated with a flash triggered from a 14 m tall structure with a discontinuous current path to ground. The UCPL lengths in this study are also shorter than the inferred return stroke initiation heights estimated by *Wang et al*. [2013], which ranged from 9.7 m (±2.4 m) to 21 m (±4.6 m) above the strike object. The launcher configuration used by *Wang et al*. [2013] also differed from

the present study, consisting of a 5 m square metallic intercepting wire ring placed above the launcher and grounded to the launcher with multiple down conductors. Unfortunately, there were no high-speed video data available to corroborate the return stroke initiation heights estimated by *Wang et al*. [2013].

The average UCPL speeds in this study can be calculated assuming the UCPL duration extends from the time when the measured channel-base current deviates continuously from the system noise level during the downward leader propagation to the initial large increase in channel-base current associated with the leader burst. By this criteria, the calculated average speeds of the UCPLs for the three events are 2.9×10^5 m/s, 3.3×10^5 m/s, and 3.0×10^5 m/s. The UCPL speeds are nearly 2 orders of magnitude slower than those reported by *Wang et al*. [1999]. If the speeds are recalculated using only the time duration of the UCPLs that are clearly visible in the high-speed video records, at most 3.08 μs, the lower bound UCPL speeds for the three events are 1.3×10^6 m/s, 2.3×10^6 m/s, and 6.5×10^5 m/s, in better agreement with *Wang et al*. [1999]. It is likely that the ALPS photodiode system used by *Wang et al*. [1999], like the high-speed camera used in this study, lacked the amplitude and spatial resolution to resolve the UCPLs except for the time period within a few microseconds of the return stroke. These combined observations help to explain why no photographs of UCPLs appear in the literature in response to naturally occurring subsequent strokes. Successfully, photographing these discharges requires microsecond-level exposure time to isolate the UCPL from the subsequent return stroke, high sensitivity to detect the faintly luminous structure, and submeter spatial resolution to resolve the short length of the discharge process.

The leader burst process was a consistently occurring waveform feature in each of the three cases shown in section 3. These combined data have shown that the leader burst is a distinctly different process than the prior downward leader steps and, without exception, is time correlated with the initial interactions of the downward and upward leader streamer zones. The leader burst is associated with the first large upward transition in channel-base current, typically from a background level of tens of amperes to many hundreds of amperes. Additionally, the current increases time coincident with the leader burst pulses without the observed time delay of the current peaks associated with the earlier downward leader steps (Figures 3, 6, and 9). The leader burst d*E*/d*t* pulse peaks were TOA located within or immediately above the connection region between the downward and upward leaders, as determined by high-speed and high-definition video records. The TOA locations of the leader burst pulse peaks in this study did not descend rapidly like those reported by *Howard et al*. [2010]. While the timing of the optical pulse relative to the slow front reported by *Wang et al*. [2001] might suggest the pulse was associated with the leader burst process, the altitude of the pulse (35 m) relative to the tip of the UCPL (88 m) is contradictory to the observations of this study which place the leader burst pulses within the immediately vicinity of the connection region between the upward and downward leaders.

Pulses superimposed on the d*E*/d*t* slow front were recorded for each of the three events detailed in section 3. The slow-front pulses occurred during the fast ramp of the channel-base current and subsequently were associated with rapid increases in the current with amplitudes ranging from several hundred amperes to nearly 7 kA. The fast-transition d*E*/d*t* pulses followed the final dominant slow-front d*E*/d*t* pulses in the three events by 740 ns, 260 ns, and 200 ns, respectively, and were associated with increases in the measured current levels by many kiloamperes in each case. The results of this study provide convincing evidence for the hypotheses provided by *Murray et al*. [2005], *Jerauld et al*. [2007], and *Howard et al*. [2010] that the slow front and fast-transition pulses are not distinctly different physical processes. In this study, both slow-front and fast-transition pulses have been shown to be associated with rapid increases in the channel-base current. It is likely that the multiple slow-front and fast-transition pulses recorded during the attachment process of a single dart-stepped leader are associated with consecutive, discrete connections of the upward and downward leaders that are confined to a relatively small spatial region. The high-speed photographic equipment used in this study lacks the combination of temporal resolution, spatial resolution, and dynamic range to successfully image these individual connections. The complex branching structure of the upward and downward leaders shown in the 30 ms exposure of Event 1 in Figure 2b provides perhaps the most compelling evidence for this phenomenon.

The observed time delay between the d*E*/d*t* and d*I*/d*t* peaks associated with both the slow-front pulses and fast-transition pulse has been previously documented by *Leteinturier et al*. [1990] for triggered lightning strokes in Florida. *Leteinturier et al*. [1990] reported an average delay between the d*E*/d*t* and d*I*/d*t* peaks of about 54 ns, accounting for the propagation delay from the triggered lightning channel base to the d*E*/d*t* sensor located at a distance of 50 m. The authors concluded that the observed delay was characteristic of

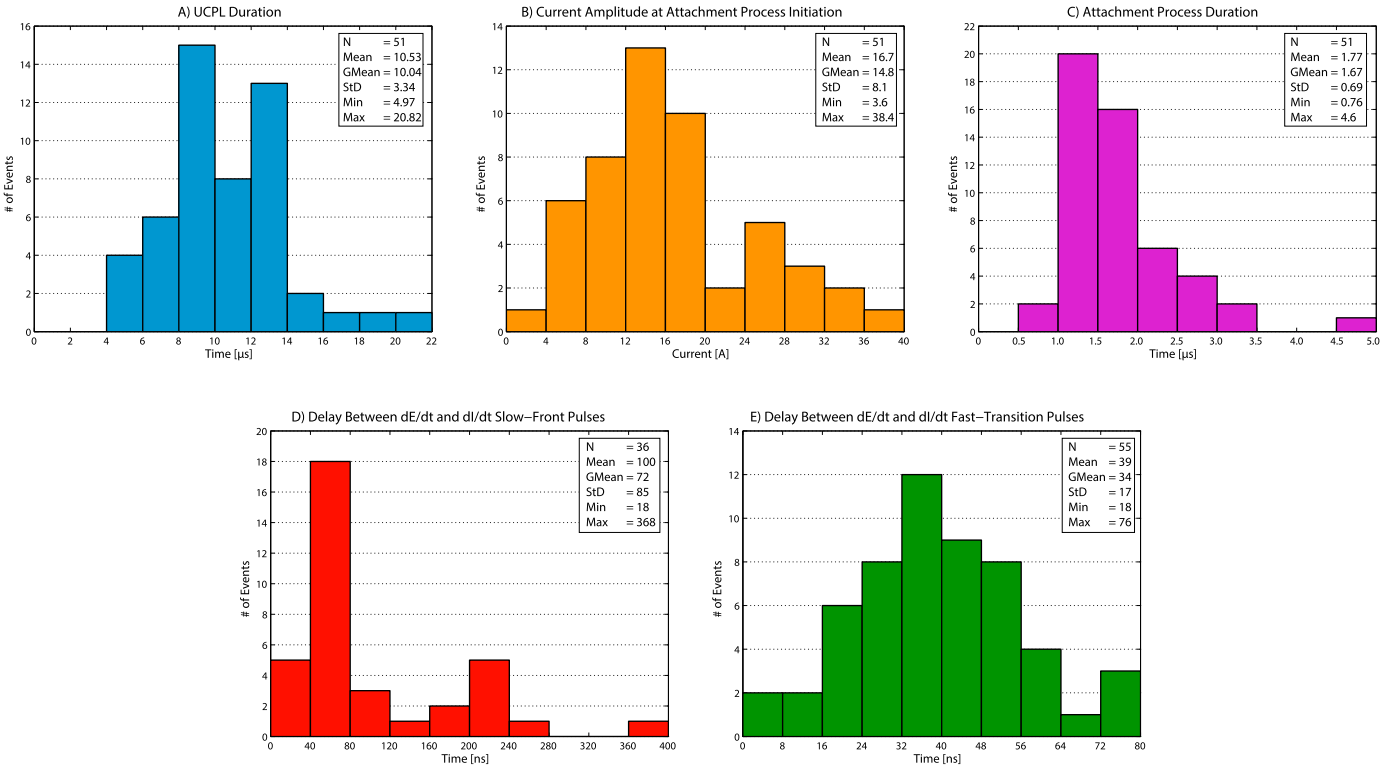

Figure 11. Histograms and summary statistics for (a) UCPL durations of 51 dart-stepped leader events, (b) current amplitudes at attachment process initiation for 51 dart-stepped leader events, (c) attachment process time durations for 51 dart-stepped leader events, (d) time delays between d*E*/d*t* and d*I*/d*t* peaks for 36 slow-front pulses, and (e) time delays between d*E*/d*t* and d*I*/d*t* peaks for 55 fast-transition pulses.

the return stroke initiating from an elevated junction point. Both *Leteinturier et al*. [1990] and *Jerauld et al*. [2007] were able to better reproduce the fine structure of the measured electric fields by incorporating a two wave TL model, in which current waves are injected at an elevated source and propagated both downward and upward. In their models, *Leteinturier et al*. [1990] and *Jerauld et al*. [2007] used downward current wave propagation speeds of 2.46×10^8 m/s and 1.55×10^8 m/s, respectively. With junction altitudes determined from high-speed and high-definition video records with accuracy better than 1 m for the three events analyzed in section 3, the average calculated downward current wave propagation speeds in this study ranged from 4.3×10^7 m/s to 1.6×10^8 m/s. These downward current wave speed estimates are in good agreement with the range reported by *Wang et al*. [2013] for downward luminosity speed, 7.0×10^7 m/s to 1.9×10^8 m/s, for three triggered lightning dart-stepped leaders at the ICLRT.

5. Statistical Analyses

Channel-base currents and d*E*/d*t* data were obtained for a total of 51 dart-stepped leaders during the summers of 2013 and 2014, three of which were analyzed in detail in section 3. Although the junction altitude could only be accurately determined (less than 1 m uncertainty) for a small subset of these data due to the availability and quality of the high-speed video recordings, such parameters as UCPL duration, UCPL current level at attachment process initiation, full attachment process duration, and the timing relationship of the d*E*/d*t* and d*I*/d*t* peaks for both slow-front and fast-transition pulses could be computed for all events. As stated previously, the UCPL duration is measured as the time between the point where the channel-base current elevates permanently from the system noise to the fast increase in current associated with the initial interaction of the upward and downward leader streamer zones at the time of the leader burst. The UCPL current at the time of attachment process initiation is measured as the current amplitude at the point where the current initially ascends rapidly. The attachment process duration is measured as the time between the initial fast increase in current associated with the leader burst and the final fast-transition d*I*/d*t* peak, which can be taken to signify that the full connection is complete. Histograms of the measured parameters are shown in Figure 11. UCPL durations (Figure 11a) ranged from

4.97 μs to 20.82 μs with a mean of 10.53 μs (geometric mean of 10.04 μs). The associated UCPL currents at the initiation of the attachment process (Figure 11b) ranged from 3.6 A to 38.4 A with a mean of 16.7 A (geometric mean of 14.8 A). The full duration of the attachment process (Figure 11c) varied from 0.76 μs to 4.6 μs with a mean of 1.77 μs (geometric mean of 1.67 μs). The outlying data point at 4.6 μs occurred with the fifth return stroke of flash UF 13–33, which also had the largest peak current (nearly 29 kA) of any stroke in the data set.

A total of 36 slow-front pulses and 55 fast-transition pulses were recorded. Four strokes exhibited two fast-transition peaks in close time-succession. The mean time delay between the d*E*/d*t* and d*I*/d*t* peaks for slow-front pulses was 100 ns (geometric mean of 72 ns) with a range from 18 ns to 368 ns (Figure 11d). The mean delay between the fast-transition d*E*/d*t* and d*I*/d*t* peaks was only 39 ns (geometric mean of 34 ns) with a range from 18 ns to 76 ns (Figure 11e). If the slow-front and fast-transition pulses are radiated from similar spatial locations, as suggested by *Howard et al*. [2010], then the downward propagating current waves associated with slow-front pulses are typically slower than those associated with fast-transition pulses by a factor of 2 to 2.5. For events with multiple slow-front pulses, the delays between the d*E*/d*t* and d*I*/d*t* peaks tended to decrease with time while the amplitudes of the slow-front pulses tended to increase with time. The mean time delay for the 55 fast-transition pulses measured in this study was about 28% less than the 54 ns value reported by *Leteinturier et al*. [1990] for Florida triggered strokes. The current path between the strike object and the current measurement device in the launcher used by *Leteinturier et al*. [1990] was about 16 m (about 11 m longer than this study) providing a delay of 53 ns assuming speed of light propagation. Thus, many of events reported by *Leteinturier et al*. [1990] likely did not have associated UCPLs and elevated junction points above the strike object. Given the results of this study, which show optically short but clearly evident UCPLs with triggered lightning dart-stepped leaders, it is likely that a high percentage of the return strokes studied by *Leteinturier et al*. [1990] were preceded by dart leaders.

6. Related Comments

The dominant d*E*/d*t* pulses associated with the final leader steps prior to the initiation of the attachment process were located via the TOA technique for Events 1, 2, and 3. For the first time, the altitudes of these impulsive radiation sources, which were determined with altitude uncertainties on the order of 1 m, were correlated with 1.54 μs high-speed video frame data. In all cases, the locations of the dominant d*E*/d*t* pulse peaks of the leader steps were located at or immediately below the ending point in space of the prior step, or more specifically, where the bidirectional propagating space leader(s) contacted the above leader channel tip. The implications of this observation are important both for understanding the evolution of the step formation process and for understanding the spatial and temporal relationship between the d*E*/d*t* pulses that signify the step formation and the related emission of X-rays. Most dart-stepped leader steps exhibit a complex d*E*/d*t* signature that includes multiple pulses within the time span of about a microsecond [e.g., *Gamerota et al*., 2014a]. An in-depth study is warranted to explore whether the earlier pulses in the step formation correspond to the evolution of the space stem/space leader process, which from correlated high-speed video records is shown to occur beneath the location of the prior leader channel tip and beneath the source location of the dominant d*E*/d*t* pulse within each step. For 15 d*E*/d*t* and X-ray source location pairs associated with triggered lightning dart-stepped leaders, *Hill et al*. [2012] recently reported that the X-ray sources were displaced vertically from the correlated d*E*/d*t* sources by about 20 m. From both laboratory experiments and the observed time separation between the d*E*/d*t* and X-ray source pairs [e.g., *Hill*, 2012], the X-rays are thought to be produced in the high-field region that occurs following the formation of the leader step when the potential of the newly formed section of channel is transferred downward, producing a burst of corona streamers beneath the ending point in space of the step. With the dominant d*E*/d*t* pulse in each step located at the top of the connection region, the actual distance between the X-ray sources and the causative leader step is shorter by the length of the previous step, which for triggered dart-stepped leaders, is typically on the order of 5–10 m [e.g., *Idone and Orville*, 1984; *Gamerota et al*., 2014a]. *Gamerota et al*. [2015] recently reported that the corona streamers propagate, on average, 9 m beneath the tips of triggered lightning dart-stepped leaders. Considering the typical step lengths and the lengths of the corona streamers following each step, the 20 m vertical displacement of the X-ray and d*E*/d*t* sources reported by *Hill* [2012] places the X-rays sources near the tip of the corona streamer zone below each step.

7. Conclusion

The attachment processes of three triggered lightning dart-stepped leader events have been analyzed using time-correlated 1.54 μs high-speed video frames supplemented by channel-base current, d*I*/d*t*, and d*E*/d*t* measurements. UCPLs associated with the three events were shown to have time durations of 13.6 μs, 21.1 μs, and 6.6 μs with final lengths of 4 m, 7 m, and 2 m, respectively. Prominent leader burst pulses were identified at the beginning of the d*E*/d*t* slow-front period for all three events. Leader burst pulses were time correlated with the first large increases in channel-base current associated with the initial interactions of the upward and downward leader streamer zones. TOA locations of the leader burst pulses were found to occur within or immediately above the connection region between the upward and downward leaders. Large-amplitude pulses superimposed on the d*E*/d*t* slow front were identified for all three events after the initial interaction between the upward and downward leaders and were associated with fast increases in the channel-base current from hundreds of amperes to many kilo-amperes. The results of this study suggest that both slow-front and fast-transition pulses are likely radiated due to individual connections between the upward and downward leaders within the attachment region. For a total of 51 dart-stepped leader events recorded during 2013 and 2014, time delays were observed and measured between the d*E*/d*t* and d*I*/d*t* peaks for 36 slow-front pulses (geometric mean time delay of 72 ns) and 55 fast-transition pulses (geometric mean time delay of 34 ns), verifying the existence of an elevated junction point between the upward and downward leaders. For the three dart-stepped leader events analyzed in detail in this paper, the downward current wave speeds from the junction heights, as determined by the high-speed video recordings, ranged from 4.3×10^7 m/s to 1.6×10^8 m/s. Average downward current wave speeds for fast-transition pulses were found to be a factor of 2 to 2.5 faster than those for slow-front pulses. For the data set of 51 dart-stepped leader events, the mean duration of the attachment process, beginning with the initial rapid current increase and terminating at the peak of the final d*I*/d*t* fast-transition pulse, was 1.77 μs.

Acknowledgments
This research was primarily funded by the DARPA NIMBUS program with additional support from NASA. The authors would also like to thank R. Wilkes for his assistance in the data collection effort. For data requests, contact Martin Uman (uman@ece.ufl.edu).

References

Berger, K., and E. Vogelsanger (1969), New results of lightning observations, in *Planetary Electrodynamics*, pp. 489–510, Gordon and Breach, New York.

Berger, K., R. B. Anderson, and H. Kroninger (1975), Parameters of lightning flashes, *Electra*, *80*, 223–37.

Biagi, C. J., D. M. Jordan, M. A. Uman, J. D. Hill, W. H. Beasley, and J. Howard (2009), High speed video observations of rocket-and-wire initiated lightning, *Geophys. Res. Lett.*, *36*, L15801, doi:10.1029/2009GL038525.

Biagi, C. J., M. A. Uman, J. D. Hill, D. M. Jordan, V. A. Rakov, and J. Dwyer (2010), Observations of stepping mechanisms in a rocket-and-wire triggered lightning flash, *J. Geophys. Res.*, *115*, D23215, doi:10.1029/2010JD014616.

Biagi, C. J., M. A. Uman, J. D. Hill, and D. M. Jordan (2014), Negative leader step mechanisms observed in altitude triggered lightning, *J. Geophys. Res. Atmos.*, *119*, 8160–8168, doi:10.1002/2013JD020281.

Cooray, V., and S. Lundquist (1982), Characteristics of the radiation fields from lightning in Sri Lanka in the tropics, *J. Geophys. Res.*, *90*, 6099–109, doi:10.1029/JD090iD04p06099.

Cooray, V., R. Montano, and V. Rakov (2004), A model to represent negative and positive lightning first strokes with connecting leaders, *J. Electrost.*, *60*, 97–109.

Dwyer, J. R., et al. (2003), Energetic radiation produced during rocket-triggered lightning, *Science*, *299*, 694–697.

Dwyer, J. R., et al. (2004), Measurements of X-ray emission from rocket triggered lightning, *Geophys. Res. Lett.*, *31*, L05118, doi:10.1029/2003GL018770.

Dwyer, J. R., et al. (2005), X-ray bursts associated with leader steps in cloud-to-ground lightning, *Geophys. Res. Lett.*, *32*, L01803, doi:10.1029/2004GL021782.

Dwyer, J. R., M. Schaal, H. K. Rassoul, M. A. Uman, D. M. Jordan, and D. Hill (2011), High-speed X-ray images of triggered lightning dart leaders, *J. Geophys. Res.*, *116*, D20208, doi:10.1029/2011JD015973.

Eriksson, A. J. (1978), Lightning and tall structures, *Trans. South Afr. IEE*, *69*, 238–252.

Gamerota, W. R., M. A. Uman, J. D. Hill, T. Ngin, J. Pilkey, and D. M. Jordan (2014a), Electric field derivative waveforms from dart-stepped-leader steps in triggered lightning, *J. Geophys. Res. Atmos.*, *119*, 10,844–10,858, doi:10.1002/2014JD021919.

Gamerota, W. R., V. P. Idone, M. A. Uman, T. Ngin, J. T. Pilkey, and D. M. Jordan (2014b), Dart-stepped-leader step formation in triggered lightning, *Geophys. Res. Lett.*, *41*, 2204–2211, doi:10.1002/2014GL059627.

Gamerota, W. R., M. A. Uman, J. D. Hill, and D. M. Jordan (2015), Observations of corona in triggered dart-stepped leaders, *Geophys. Res. Lett.*, *42*, doi:10.1002/2014GL062911.

Gao, Y., W. Lu, Y. Ma, L. Chen, Y. Zhang, X. Yan, and Y. Zhang (2014), Three-dimensional propagation characteristics of the upward connecting leaders in six negative tall-object flashes in Guangzhou, *Atmos. Res.*, *149*, 193–203, doi:10.1016/j.atmosres.2014.06.008.

Hill, J. D. (2012), The mechanisms of lightning leader propagation and ground attachment, PhD dissertation, Univ. of Florida, Gainesville, Fla. [Available at http://ufdc.ufl.edu/UFE0044602.]

Hill, J. D., M. A. Uman, and D. M. Jordan (2011), High-speed video observations of a lightning stepped leader, *J. Geophys. Res.*, *116*, D16117, doi:10.1029/2011JD015818.

Hill, J. D., M. A. Uman, D. M. Jordan, J. R. Dwyer, and H. K. Rassoul (2012), "Chaotic" dart leaders in triggered lightning: Electric fields, X-rays, and source locations, *J. Geophys. Res.*, *117*, D03118, doi:10.1029/2011JD016737.

Howard, J., M. A. Uman, J. R. Dwyer, D. Hill, C. Biagi, Z. Saleh, J. Jerauld, and H. K. Rassoul (2008), Co-location of lightning leader X-ray and electric field change sources, *Geophys. Res. Lett.*, *35*, L13817, doi:10.1029/2008GL034134.

Howard, J., M. A. Uman, C. Biagi, D. Hill, J. Jerauld, V. A. Rakov, J. Dwyer, Z. Saleh, and H. Rassoul (2010), RF and X-ray source locations during the lightning attachment process, *J. Geophys. Res.*, *115*, D06204, doi:10.1029/2009JD012055.

Howard, J., M. A. Uman, C. Biagi, D. Hill, V. A. Rakov, and D. M. Jordan (2011), Measured close lightning leader-step electric field–derivative waveforms, *J. Geophys. Res.*, *116*, D08201, doi:10.1029/2010JD015249.

Idone, V. P., and R. E. Orville (1984), Three unusual strokes in a triggered lightning flash, *J. Geophys. Res.*, *89*(D5), 7311–7316, doi:10.1029/JD089iD05p07311.

Jerauld, J., M. A. Uman, V. A. Rakov, K. J. Rambo, and G. H. Schnetzer (2007), Insights into the ground attachment process of natural lightning gained from an unusual triggered-lightning stroke, *J. Geophys. Res.*, *112*, D13113, doi:10.1029/2006JD007682.

Jerauld, J., M. A. Uman, V. A. Rakov, K. J. Rambo, D. M. Jordan, and G. H. Schnetzer (2008), Electric and magnetic fields and field derivatives from lightning stepped leaders and first return strokes measured at distances from 100 to 1000 m, *J. Geophys. Res.*, *113*, D17111, doi:10.1029/2008JD010171.

Jiang, R., X. Qie, M. Liu, G. Lu, Z. Wang, Z. Sun, X. Wu, H. Zhang, K. Liu, and X. Li (2014), High speed video observation of lightning attachment process and the associated leader behaviors, XV International Conference on Atmospheric Electricity. [Available at http://www.nssl.noaa.gov/users/mansell/icae2014/preprints/Jiang_118.pdf.]

Leteinturier, C., C. Weidman, and J. Hamelin (1990), Current and electric field derivatives in triggered lightning return strokes, *J. Geophys. Res.*, *95*(D1), 811–828, doi:10.1029/JD095iD01p00811.

Lu, W., L. Chen, Y. Ma, V. A. Rakov, Y. Gao, Y. Zhang, Q. Yin, and Y. Zhang (2013), Lightning attachment process involving connection of the downward negative leader to the lateral surface of the upward connecting leader, *Geophys. Res. Lett.*, *40*, 5531–5535, doi:10.1002/2013GL058060.

Murray, N. D., E. P. Krider, and J. C. Willett (2005), Multiple pulses in dE/dt and the fine structure of E during the onset of first return strokes in cloud-to-ocean lightning, *Atmos. Res.*, *76*, 455–480.

Orville, R. E., and V. P. Idone (1982), Lightning leader characteristics in the Thunderstorm Research International Program (TRIP), *J. Geophys. Res.*, *87*, 11,177–11,192, doi:10.1029/JC087iC13p11177.

Petersen, D. A., and W. H. Beasley (2013), High-speed video observations of a natural negative stepped leader and subsequent dart-stepped leader, *J. Geophys. Res. Atmos.*, *118*, 12,110–12,119, doi:10.1002/2013JD019910.

Rakov, V. A., and M. A. Uman (2003), *Lightning: Physics and Effects*, Cambridge Univ. Press, Cambridge, U. K.

Saleh, Z., J. Dwyer, J. Howard, M. Uman, M. Bakhtiari, D. Concha, M. Stapleton, D. Hill, C. Biagi, and H. Rassoul (2009), Properties of the X-ray emission from rocket-triggered lightning as measured by the Thunderstorm Energetic Radiation Array (TERA), *J. Geophys. Res.*, *114*, D17210, doi:10.1029/2008JD011618.

Schaal, M. M., J. R. Dwyer, H. K. Rassoul, J. D. Hill, D. M. Jordan, and M. A. Uman (2013), The angular distribution of energetic electron and X-ray emissions from triggered lightning leaders, *J. Geophys. Res. Atmos.*, *118*, 11,712–11,726, doi:10.1002/2013JD019619.

Schaal, M. M., et al. (2014), The structure of X-ray emissions from triggered lightning leaders measured by a pinhole-type X-ray camera, *J. Geophys. Res. Atmos.*, *119*, 982–1002, doi:10.1002/2013JD020266.

Thottappillil, R., and M. A. Uman (1993), Comparison of return stroke models, *J. Geophys. Res.*, *98*(D12), 22,903–22,914, doi:10.1029/93JD02185.

Tran, M. D., V. A. Rakov, and S. Mallick (2014), A negative cloud-to-ground flash showing a number of new and rarely observed features, *Geophys. Res. Lett.*, *41*, 6523–6529, doi:10.1002/2014GL061169.

Uman, M. A., and D. K. McLain (1969), Magnetic field of the lightning return stroke, *J. Geophys. Res.*, *74*(28), 6899–6910, doi:10.1029/JC074i028p06899.

Visacro, S., A. Soares Jr., M. A. O. Schroeder, L. C. Cherchiglia, and V. J. de Sousa (2004), Statistical analysis of lightning current parameters: measurements at Morro do Cachimbo Station, *J. Geophys. Res.*, *109*, D01105, doi:10.1029/2003JD003662.

Wang, D., V. A. Rakov, M. A. Uman, N. Takagi, T. Watanabe, D. E. Crawford, K. J. Rambo, G. H. Schnetzer, R. J. Fisher, and Z. I. Kawasaki (1999), Attachment process in rocket triggered lightning strokes, *J. Geophys. Res.*, *104*(D2), 2143–2150, doi:10.1029/1998JD200070.

Wang, D., M. Chen, N. Takagi and T. Watanabe (2001), Correlated Sub-microsecond E-field and High-Speed Image of the Natural Lightning Attachment Process, SAE Tech. Pap. 2001-01-2882, doi:10.4271/2001-01-2882.

Wang, D., N. Takagi, W. R. Gamerota, M. A. Uman, J. D. Hill, and D. M. Jordan (2013), Initiation processes of return strokes in rocket-triggered lightning, *J. Geophys. Res. Atmos.*, *118*, 9880–9888, doi:10.1002/jgrd.50766.

Warner, T. A. (2010), Upward leader development from tall towers in response to downward stepped leaders, in *30th International Conference on Lightning Protection*, 1069, Power and Energy Soc, Cagliari, Italy.

Weidman, C. D., and E. P. Krider (1978), The fine structure of lightning return stroke wave forms, *J. Geophys. Res.*, *83*(C12), 6239–6247, doi:10.1029/JC083iC12p06239.